Available online at www.sciencedirect.com
SCIENCE DIRECT
Cement and Concrete Research 36 (2006) 1330–1344
Cement and Concrete Research

Influence of inclusion shapes on the effective linear elastic properties of hardened cement pastes

E. Stora [a,b,*], Q.-C. He [a], B. Bary [b]

[a] Laboratoire de Mécanique, Université de Marne la Vallée, 5 bd. Descartes 77454 Marne-la-Vallée Cedex 2, France
[b] Atomic Energy Commission, Laboratoire d'Etude du Comportement des Bétons et des Argiles, 91191 Gif/Yvette, France

Received 18 August 2005; accepted 4 February 2006

Abstract

In most micromechanical models applied to cement pastes, particulate phases are modeled as spheres. However, experimental observations clearly show that certain of them are far from being spherical. The present work focuses on the effects of particle phase shapes on the effective isotropic linear elastic moduli of hardened cement pastes (HCP). An attempt to develop a more realistic micromechanical model is proposed by using spheroidal inclusions and including a novel morphological parameter. The latter is identified on the basis of experimental result issue for example from microtomographic images of Portland cement grains. With the help of the proposed model, the validity range of spherical particulate approximations is examined for both sound and leached pastes.

Keywords: Microstructure; Elastic moduli; Micromechanics; Cement paste; Modeling

1. Introduction

Micromechanical models aim at predicting the effective macroscopic properties of a heterogeneous material from the knowledge of the geometric and physical characteristics of its various microstructural components. Their application to estimating the isotropic linear elastic effective properties of cement pastes is relatively recent. A homogenization attempt for tricalcium silicate (C_3S) pastes was performed in 1997 by Neubauer et al. [1] using the differential scheme but mechanical input values for the calcium–silicate–hydrates (C–S–H) phase were lacking. Owing to progress in experimental mechanics, elastic properties of all the main phases present in hardened cement pastes (HCP) are nowadays measurable by nanoindentation techniques and many data may be found in the literature [2–6]. Benefiting from these recent nanoindentation measures, an efficient two-step homogenization procedure for HCP on the basis of the Mori-Tanaka model (MT) has been developed by Constantinides and Ulm [2]. Their Young modulus estimations for both sound and leached Type I Ordinary Portland Cement (OPC) pastes with water–cement ratio $w/c=0.5$ showed good agreement with experimental results. Bernard and al. [7] used the same two-scale description of microstructure and the self-consistent scheme to study early-age cement pastes and predict the solid phase percolation during hydration process. They also obtained results consistent with experimental values.

The scope of the present paper is to investigate the possibility of improving on these upscaling models by integrating some significant information about the shapes of HCP particulate phases. In the models cited above [1,2,7], all inclusion phases are systematically approximated by spheres for simplicity, though cement paste micrographs indicate that none of these phases is really spherical. The present article assesses the validity range of the spherical particulate assumption for HCP. For this purpose, we study how the HCP effective linear elastic properties change with the inclusion geometry. We demonstrate that they actually vary significantly in some cases, for which more realistic geometric forms should be applied.

Though volume fractions and mechanical data of the main phases composing HCP are now determined in a relatively precise way, less is known concerning their morphology. Based

* Corresponding author. Laboratoire de Mécanique, Université de Marne-la-Vallée, 19 rue A. Nobel, F-77420 Champs sur Marne, France. Tel.: +33 1 60 95 77 94.
E-mail address: stora@univ-mlv.fr (E. Stora).

0008-8846/$ - see front matter © 2006 Elsevier Ltd. All rights reserved.
doi:10.1016/j.cemconres.2006.02.007

on relevant experimental results, an attempt to approach the components real shapes by means of a morphological parameter is made. Although the breakthrough of three-dimensional analysis techniques provides some interesting data, the introduction of realistic particle shapes in homogenization models is still a difficult task. It is generally impossible to incorporate the phase real morphologies directly in micromechanical methods and approximations of these shapes by simpler geometrical forms are necessary. The dilemma is to integrate the most realistic shapes possible and at the same time conserve a calculable model. An analytical solution is proposed in the present homogenization approach by introducing spheroids adequately chosen with the help of the previously mentioned morphological parameter.

The paper is organized as follows. Section 2 details the main steps in the present homogenization process. A generalization of the previous two-scale model for HCP [2] is proposed on the basis of spheroidal inclusions and of the Interaction Direct Derivative estimate (IDD) [8]. In Section 3, the cases for which morphology actually plays a significant role on elastic macroscopic properties are rigorously investigated. In addition, an efficient morphological parameter is introduced to characterize the inclusion shapes. The spheroids representing the particulate phases in the micromechanical approach are then determined through this parameter. In Section 4, this novel homogenization model is applied to a representative panel of sound and leached HCP and its estimations are respectively compared with the effective elastic properties obtained by the approach of Constantinides and Ulm [2] and by the finite element (FE) method [9].

2. Micromechanical model

The micromechanical analysis presented in this section is concerned with the microstructure of HCP and based on the model proposed by Zheng and Du [8]. The latter is particularly suited for accounting for the effects of non-spherical morphology on effective isotropic properties. As every complete micromechanical analysis, the one given below comprises three parts: representation, localization and homogenization [10].

2.1. HCP microstructure

A detailed investigation of HCP microstructure is primarily required to build a realistic homogenization model. In particular, we need to specify the involved phases and their mechanical properties, distributions, sizes and shapes. HCP form due to hydration of cement grains. The reaction of cement particles with water initially takes place at the particle surface. Consequently, cement grain shapes play an important role in the HCP properties. The main hydration products are: C–S–H, Portlandite or calcium hydroxide (CH) and aluminates. It is now commonly accepted that there are two types of C–S–H. Jennings and Tennis classified them as high-density and low-density, whereas Richardson preferred to call them inner and outer products [11–13]. In the following, the two types of C–S–H are denoted C–S–H^{int} and C–S–H^{ext}. Both phases of C–S–H contain nanopores and can even enclose nanoparticles of CH or aluminates. Nevertheless, both phases can be considered as homogeneous materials with elastic properties which may be identified by nanoindentation technique [2].

The characteristic sizes of the phases composing HCP range from the nanometer to micrometer scales. The heterogeneity of HCP thus manifests itself at different scales. Constantinides and Ulm [2] distinguish two microstructural levels respecting the scales separation condition: the first ranging from 10 nanometers to 0.1 μm is characteristic of the two types of C–S–H, while the second varying from 1 μm to 100 μm corresponds to the scale where C–S–H can be regarded as a homogeneous matrix with CH crystals, capillary pores, anhydrous residuals and aluminates as inclusions. The first step consists in calculating C–S–H matrix effective properties from C–S–H^{int} and C–S–H^{ext} intrinsic values and the second one is to determine HCP effective properties with the aid of the previous result for C–S–H matrix. However, according to some authors [13–15], the distinction between C–S–H^{int} and C–S–H^{ext} should be done only at level II since these phases form successively from cement grain surfaces, the C–S–H^{int} resulting mainly from higher confinement conditions and from water accessibility during hydration reactions. Nevertheless, for the sake of simplicity the homogenization model presented here adopts the two-scale microstructure [2,7].

At level I, The C–S–H matrix behaves as a heterogeneous material with an inclusion-matrix type microstructure. The C–S–H^{ext} plays the role of a matrix phase, surrounding the C–S–H^{int} as inclusion. As already mentioned, this latter phase has a characteristic size of 10^{-8} to 10^{-7} m, which makes it very difficult to gain precise information about its geometrical shape. Thus, the spherical form is adopted for C–S–H^{int} by Constantinides and Ulm [2], though Taylor [14] describes it as a honeycomb or reticular network.

At level II, the main phases are the homogenized C–S–H, CH crystals, capillary pores (V), unhydrated Clinker (UC), Ettringite or alumino-ferrite (AFt) and monosulfoaluminates (AFm). Precisely, the C–S–H acts as a matrix phase in which the other phases are embedded and play the role of inclusion. An experimentally based description of the morphology of these inclusions constitutes a preliminary for a physically sound micromechanical modeling. Based on some relevant experimental results, an attempt is performed below to provide such a description.

- CH crystals (Portlandite): they are often described as platelets or flakes when embedded in HCP [13]. Otherwise in non-confined environment, Portlandite crystallizes into massive hexagonal plates. Recently, Diamond [16] by means of backscatter-mode scanning electron microscopy pointed out the fact that CH appears as irregular masses. These observations are also confirmed by the Visible Cement Data Set [17]. Consequently, they seem far from being spherical, although information on CH crystals in HCP is insufficient to quantitatively confirm this observation.
- Aluminates: according to Richardson [13], AFm is present in mature pastes as large irregular plates similar to those of CH.

Ettringite forms during hydration process as thin hexagonal prism needles of up to 10 μm in length. AFt is quite easy to observe on environmental scanning electron microscopy (ESEM), since they are usually characterized by long rods when crystallized in non-confined environment.

- Unhydrated Clinker: it corresponds to the portion of cement grains that has not reacted with water. The amount of anhydrous residuals present in HCP depends on *w*/*c*. Cement paste micrographs generally tend to show that cement particles do not have spherical shapes. With the help of advanced techniques such as X-ray microtomography, cement particle morphology has been successfully investigated. Garboczi and Bullard [18], recently performing a spherical harmonic coefficient analysis on microtomographic images of Portland cement grains, were able to characterize quantitatively their real shape. They analyzed about 1200 particles with volume ranging from 1 μm^3 to 120,000 μm^3 and plotted their true surface area A versus their volume V. By fitting this wide data collection they obtained the following result [18]:

$$A = 8V^{0.64}. \tag{1}$$

  They further noticed that this formula differs clearly from the spherical one $A_{\text{sphere}} = 4.84\, V^{2/3}$, thus showing the asphericity of cement particles. The experimental results about the ratio between the surface area and volume of real cement particles are precious information that will be further exploited in Section 3.
- Initial capillary pores: they are originated from chemical shrinkage of the hydration products or stem from the interstitial space left by water in excess. Their typical morphology is very difficult to characterize. However, the recent microtomographic images of Rattanasak and Kendall [19] and of the Visible Cement Data Set [17] could give some insights on their three-dimensional shapes.

The previous discussions highlight the asphericity of all the hydrated phases and unhydrated Clinker. Hence, it is natural to pose the following question: what is the error induced by the spherical shape approximation of the inclusions in HCP with respect to the homogenized isotropic elastic properties? An answer to this question will be provided in Section 3.

2.2. Localization

In the foregoing discussion, it is pointed out that HCP exhibits a two-level microstructure. Each level can be represented by a representative volume element (RVE) composed of a matrix phase, indexed by M, and of m particulate phases, which are assumed to be individually homogeneous and isotropic. Their compliance tensors are respectively denoted by $\mathbf{S}^M$ and $\mathbf{S}^r$ ($r=1, \ldots, m$). Each particulate phase r consists of inclusion particles V_j^r ($j=1, \ldots, n_r$) that are of same shape but can be of different sizes or orientations. Let V be the domain occupied by an RVE of the heterogeneous material at one of the two levels and let V^r correspond to the sub-domain of inclusion phase r (where respectively $r=\text{C–S–H}^{\text{int}}$ for level I and $r=$CH, UC, V, AFt and AFm for level II). In what follows, we designate the boundary surface of V by ∂V and the volume fraction of phase r by c_r.

The RVE is subjected to uniform boundary tractions over its surface ∂V:

$$\boldsymbol{t}_n = \boldsymbol{\sigma}^{\infty}\boldsymbol{n} \text{ on } \partial V, \tag{2}$$

where $\boldsymbol{t}_n$ denotes the traction vector, $\boldsymbol{n}$ designates the outward normal unit vector to the surface ∂V and $\boldsymbol{\sigma}^{\infty}$ is a constant stress tensor. The macroscopic stress tensor $\bar{\boldsymbol{\sigma}}$ is defined as the volume average $\langle\boldsymbol{\sigma}\rangle$ of the microscopic one $\boldsymbol{\sigma}$ over V and can be shown to be equal to $\boldsymbol{\sigma}^{\infty}$ [10]. In linear elasticity, this macroscopic stress tensor $\bar{\boldsymbol{\sigma}}$ and the volume average $\bar{\boldsymbol{\sigma}}_r=\langle\boldsymbol{\sigma}\rangle$ of $\boldsymbol{\sigma}$ over a particulate phase V_r are related by a fourth-order tensor $\mathbf{B}_r$ called "concentration factor":

$$\bar{\boldsymbol{\sigma}}_r = \mathbf{B}_r\bar{\boldsymbol{\sigma}}. \tag{3}$$

In the case of random heterogeneous materials, $\mathbf{B}_r$ is very difficult to determine and approximations for $\mathbf{B}_r$ are required. The dilute model provides a simple expression for these tensors. It considers the ideal situation where a single inclusion V_I^r, having the same shape as phase r, is embedded in an infinite matrix medium subjected to a uniform far-field stress. The determination of these dilute concentration factors is achieved by means of the equivalent homogeneous inclusion method [20,21]. They can be expressed as follows:

$$\mathbf{B}_r^d = \left[\mathbf{I} + \boldsymbol{\Omega}_r^M\mathbf{H}_r\right]^{-1} \text{ with } \boldsymbol{\Omega}_r^M = \mathbf{C}^M\left(\mathbf{I} - \boldsymbol{\Sigma}_r^M\right), \tag{4}$$

where $\mathbf{C}^M=(\mathbf{S}^M)^{-1}$ is the matrix stiffness tensor and $\boldsymbol{\Sigma}_r^M$ denotes the Eshelby tensor of the single inclusion V_I^r embedded in the matrix. The eigenstiffness tensor $\boldsymbol{\Omega}_r^M$ used by Zheng and Du [8] has the following mechanical interpretation: when a uniform eigenstrain tensor $\boldsymbol{\varepsilon}_I^*$ is prescribed over V_I^r inside an infinite matrix medium, the average $\bar{\boldsymbol{\sigma}}_I$ of the stress $\boldsymbol{\sigma}_I$ induced by $\boldsymbol{\varepsilon}_I^*$ over V_I^r is linearly related to $\boldsymbol{\varepsilon}_I^*$ by $\boldsymbol{\Omega}_r^M$. In particular, the tensor $\boldsymbol{\Omega}_r^M$ takes into account both shape and orientation of the inclusion and the matrix material enclosing it. The determination of the eigenstiffness tensor $\boldsymbol{\Omega}_r^M$ is usually quite complicated for non-spherical inclusions. It comes from the fact that the Eshelby tensor $\boldsymbol{\Sigma}_r^M$ generally has to be estimated numerically except for some simple cases. In particular, the Eshelby tensor of spheroids presents the benefit of being analytically calculable [22]. That is why all inclusion phases are approximated by spheroids in our homogenization process. The reader should refer to [23,24] for further information on the use of more complex shapes.

The validity range of the dilute concentration factor $\mathbf{B}_r^d$ is very limited, since all the particles are required to be far enough from each other, so as to be regarded as isolated. More advanced schemes trying to reflect the interaction effects between inclusions are required. MT effective medium approximation may be used for this purpose. Benveniste [25] has proposed an elegant reformulation of this estimate, where it can be seen as an

improved dilute model. More precisely, the stress applied at infinity is no longer $\boldsymbol{\sigma}^{\infty}$ but is replaced by the average $\overline{\boldsymbol{\sigma}}_M$ of the microscopic stress $\boldsymbol{\sigma}$ inside the matrix. It thus takes into account the stress perturbation inside the matrix phase due to the presence of the other inclusions. The concentration factors for the MT scheme are expressed as follows [25]:

$$\mathbf{B}_r^{MT} = \mathbf{B}_r^d \left[\mathbf{I} - \sum_i c_i \mathbf{H}_i \boldsymbol{\Omega}_i^M \mathbf{B}_i^d \right]^{-1}. \tag{5}$$

These concentration factors are more realistic than the dilute ones, but are not able to incorporate the influence of inclusion spatial distribution.

To circumvent this difficulty, the basic idea used in some recent homogenization methods is to model such a distribution by an ellipsoidal cell, called double-inclusion, surrounding the inclusion [8,26,27]. Its geometry depends on how the inclusions are dispersed through the matrix and thus is representative of the spatial distributions of the particulate phases. More precisely, it geometrically characterizes the probability distribution function introduced by Ponte-Castañeda and Willis [28]. The cement pastes are considered as macroscopically isotropic. Consequently, for each particulate phase of HCP, the corresponding double-inclusion should be taken as spherical. Nevertheless, for a spherical distribution of randomly oriented spheroids, highly concentrated inclusions may overlap. The maximum volume fraction for which these spheroidal inclusions do not overlap is calculated in Appendix A. For higher volume fractions, a non-spherical double-inclusion must be adopted. Once its exact shape has been determined for each particulate phase r, the eigenstiffness tensors of the various double-inclusions denoted by $\boldsymbol{\Omega}_{Dr}^M$ enclosing the inclusion V_I^r are calculated from Eq. (4). The subscript 'D' is used here, since the inclusion distribution is involved in these eigenstiffness tensors. The concentration factors $\mathbf{B}_r^{\mathrm{IDD}}$ for the IDD estimate can be obtained easily by introducing the eigenstiffness tensors of all double-inclusions and by modifying $\mathbf{B}_r^{MT}$ (see Eq. (5)) as follows [8]:

$$\mathbf{B}_r^{\mathrm{IDD}} = \mathbf{B}_r^d \left[I - \sum_i c_i \mathbf{H}_i \boldsymbol{\Omega}_{Di}^M \mathbf{B}_i^d \right]^{-1} \text{ with}$$
$$\boldsymbol{\Omega}_{Di}^M = \mathbf{C}^M \left(I - \boldsymbol{\Sigma}_{Di}^M \right). \tag{6}$$

If the inclusions are spheroids and the effective material is macroscopically isotropic, IDD and MT do not coincide. But Eqs. (5) and (6) reveal that they coincide whenever all inclusion phases V_I^r have the same eigenstiffness tensors $\boldsymbol{\Omega}_{Dr}^M = \boldsymbol{\Omega}_r^M$ as their surrounding double-inclusion. It means that every inclusion V_I^r and its enclosing cell designated by V_D^r are similar in shape and coaxial in orientation. It implies in particular that the two models coincide for macroscopically isotropic heterogeneous materials containing only spherical inclusions. Therefore the homogenization approach developed here includes the one proposed by Constantinides and Ulm [2] as a particular case.

2.3. Homogenization

The compliance tensor of the equivalent effective medium is designated by $\mathbf{S}^E$. In addition, the compliance increment H and inclusion compliance fluctuations $\mathbf{H}_r$ are defined as:

$$\mathbf{H} = \mathbf{S}^E - \mathbf{S}^M, \mathbf{H}_r = \mathbf{S}^r - \mathbf{S}^M. \tag{7}$$

The effective compliance tensor can be expressed in terms of the compliance tensors of the various phases and of the concentration factors defined by Eq. (3) (see for example [29]):

$$\mathbf{S}^E = \mathbf{S}^M + \sum_r c_r (\mathbf{S}^r - \mathbf{S}^M) \{ \mathbf{B}_r \}, \tag{8}$$

where curly brackets denote the average over all possible orientations of phase r.

By using Eq. (7), the previous relation results in:

$$\mathbf{H} = \sum_r c_r \mathbf{H}_r \{ \mathbf{B}_r \}. \tag{9}$$

This shows that the knowledge of the concentration factors of inclusion phases is sufficient to calculate the effective elastic properties. The substitution of $\mathbf{B}_r$ by its expression in Eq. (6) yields the explicit IDD estimate [8]:

$$\mathbf{H}^{\mathrm{IDD}} = \left[\mathbf{I} - \sum_r \mathbf{H}_r^d \{ \boldsymbol{\Omega}_{Dr}^M \} \right]^{-1} \mathbf{H}^d \text{ where}$$
$$\mathbf{H}^d = \sum_r \mathbf{H}_r^d \text{ and } \mathbf{H}_r^d = c_r (\mathbf{H}_r^{-1} + \{ \boldsymbol{\Omega}_r^M \})^{-1}. \tag{10}$$

In Eq. (10), $\mathbf{H}^d$ is the dilute estimate for the compliance increment. The original deductions of IDD estimate by Zheng and Du consist in consecutive applications of superposition principles. For further details, the reader should refer to the two papers from Zheng and Du [8,30]. In the present article, we have adopted the philosophy of Benveniste [25] in order to present the IDD estimate in a simple manner and to put in evidence the strong connection existing between the IDD and MT models. The demonstration proposed here shows that the IDD can be seen as an improved dilute model with unbounded matrix material subjected to the modified effective stress $\boldsymbol{\sigma}_{\mathrm{IDD}}^{\infty}$ defined as:

$$\boldsymbol{\sigma}_{\mathrm{IDD}}^{\infty} = \left[\mathbf{I} - \sum_r \mathbf{H}_r^d \{ \boldsymbol{\Omega}_{Dr}^M \} \right]^{-1} \boldsymbol{\sigma}^{\infty}. \tag{11}$$

According to Zheng and Du [8,30], the IDD estimate presents the following benefits:

- it has a simple and explicit structure;
- it is valid for multiphase composites with various inclusion geometries;
- it can properly take into account the influence of various inclusion distributions and interaction between inclusions and their immediately surrounding region.

This estimate is convenient for macroscopically isotropic materials containing non-spherical inclusions and therefore constitutes a suitable tool for studying the influence of inclusion

shapes in cementitious materials. Zheng and Du [8] verified the validity of their model in the case of a porous material containing only spherical cavities thus getting exactly the same results as MT. To the authors' knowledge, their model has never been applied to materials with spheroidal inclusions.

In particular, the IDD estimate applied to the level I of HCP microstructure gives:

$$\mathbf{H}^{\mathrm{IDD}}_{\mathrm{C-S-H}} = [\mathbf{I} - \mathbf{H}^{d}_{\mathrm{C-S-H^{int}}}\{\boldsymbol{\Omega}^{M}_{Dr}\}]^{-1}\mathbf{H}^{d}_{\mathrm{C-S-H^{int}}}. \tag{12}$$

Furthermore, the IDD estimate applied to the level II of HCP microstructure $\mathbf{H}^{\mathrm{IDD}}_{\mathrm{HCP}}$ results in:

$$\mathbf{H}^{\mathrm{IDD}}_{\mathrm{HCP}} = [\mathbf{I} - \mathbf{H}^{d}_{\mathrm{HCP}}\{\boldsymbol{\Omega}^{\mathrm{C-S-H}}_{Dr}\}]^{-1}\mathbf{H}^{d}_{\mathrm{HCP}} \tag{13a}$$

with

$$\mathbf{H}^{d}_{\mathrm{HCP}} = \sum_{r} c_r \left[\{\boldsymbol{\Omega}^{\mathrm{C-S-H}}_{r}\} + \left(\frac{1}{3K_r} - \frac{1}{3K_{\mathrm{C-S-H}}}\right)^{-1} + \mathbf{J}\left(\frac{1}{2G_r} - \frac{1}{2G_{\mathrm{C-S-H}}}\right)^{-1}\mathbf{K}\right]^{-1}, \tag{13b}$$

where r=CH, V, UC, AFt or AFm. In the last expression, **J** and **K** are respectively the hydrostatic and deviatoric operators. The bulk and shear moduli of inclusion phase r are respectively denoted by K_r and G_r. Note that the bulk and shear moduli of C–S–H matrix, respectively designated by $K_{\mathrm{C-S-H}}$ and $G_{\mathrm{C-S-H}}$, are obtained from the level I of homogenization.

3. Influence of inclusion shapes

In the previous micromechanical models applied to cement pastes [1,2,7], the basic input parameters required are the bulk moduli K_r and K_M, shear moduli G_r and G_M, and the volume fractions c_r and c_M of each phase. None of these usual parameters takes into consideration the morphology of the particulate phases. The aim of this section is to introduce a relevant parameter approximating the real shapes of inclusions.

3.1. Definition of a shape parameter for the inclusions

We propose to analyze the geometry of an inclusion by considering the ratio of its volume V over surface area A. For example, this ratio for an arbitrary spheroid can be written as:

$$\frac{V}{A} = f\left(\frac{b}{a}\right)a, \tag{14}$$

where a is the radius of the circular base of the spheroid and b is either the minor axis for oblate spheroids or the major one for prolate ones. The aspect ratio of the spheroid is designated by $r_I = b/a$. The most natural way to normalize V/A is to divide this ratio by one third of the radius R_{eq} of the equivalent sphere having the same volume V:

$$\varsigma = \frac{3V}{AR_{\mathrm{eq}}} \quad \text{with} \quad \begin{cases} \varsigma_{\mathrm{sphere}} = 1 \\ \varsigma_{\mathrm{disk}} = \varsigma_{\mathrm{needle}} = 0 \end{cases}. \tag{15}$$

This shape or morphological parameter ò has the interesting property that it varies between 0 and 1. This comes from the fact that, among all shapes, the sphere is the one that maximizes the inner volume for a given surface area according to an isoperimetric theorem [31]. The less spherical the inclusion is, the lower ς becomes. Therefore, the value of ς allows quantifying the asphericity of a particle. As an example, we calculate the morphological parameter ς of Portland cement particles with the aid of the results of Garboczi and Bullard [18]. If use is made of their fit function $A = 8V^{0.64}$, ς is not dimensionless. Consequently, we perform a new fitting of their results with a fixed exponent of 2/3 and obtain:

$$A = 5.95V^{2/3}. \tag{16}$$

The dimensionless morphological parameter ς is easily calculable from this new fit function:

$$\varsigma_{\text{cement particles}} \cong 0.81. \tag{17}$$

This value agrees with their analysis concluding that cement grains are not spherical [18]. By approximating the particle shape, ς introduces some important information on material microstructure in the elastic moduli estimate, and may be regarded as the most significant microstructural parameter after volume fractions.

In order to assess the reliability of ς, it is interesting to study if oblate and prolate spheroidal inclusions with the same shape parameter and volume fraction actually have similar effects on macroscopic elastic moduli. Hence, simulations are performed in which an arbitrary particulate phase r of HCP is approximated respectively by prolate and oblate spheroids, while the other inclusion phases are represented by spheres. The evolution of the effective elastic moduli is examined with these two types of spheroids as their parameter ς decreases from 1 to 0. Fig. 1 schematically represents the randomly oriented spheroids corresponding to an identical particulate phase r and their surrounding double-inclusions inside the RVE. For simplicity these spheroids are assumed to have the same size. The number of spheroids per unit volume is denoted by N_r. The volume fraction c_r of phase r can thus be written as:

$$c_r = N_r V_{\mathrm{spheroid}} = \begin{cases} \frac{4}{3}N_r\pi a^3 r_I & \text{for oblate spheroids} \\ \frac{4}{3}N_r\pi\frac{b^3}{r_I^2} & \text{for prolate ones} \end{cases}. \tag{18}$$

According to this equation, the variation of the aspect ratio r_I, and consequently of the shape parameter ς, of the spheroids can be performed in two different ways:

- The maximum axis of the spheroid (=a for an oblate one and b for a prolate one) varies and c_r is kept constant, as illustrated on Fig. 1 (bottom left).
- The maximum axis of the spheroid remains constant and c_r changes, as illustrated on Fig. 1 (bottom right).

For the present application, the first possibility seems more appropriate because it keeps a constant volume fraction. But it

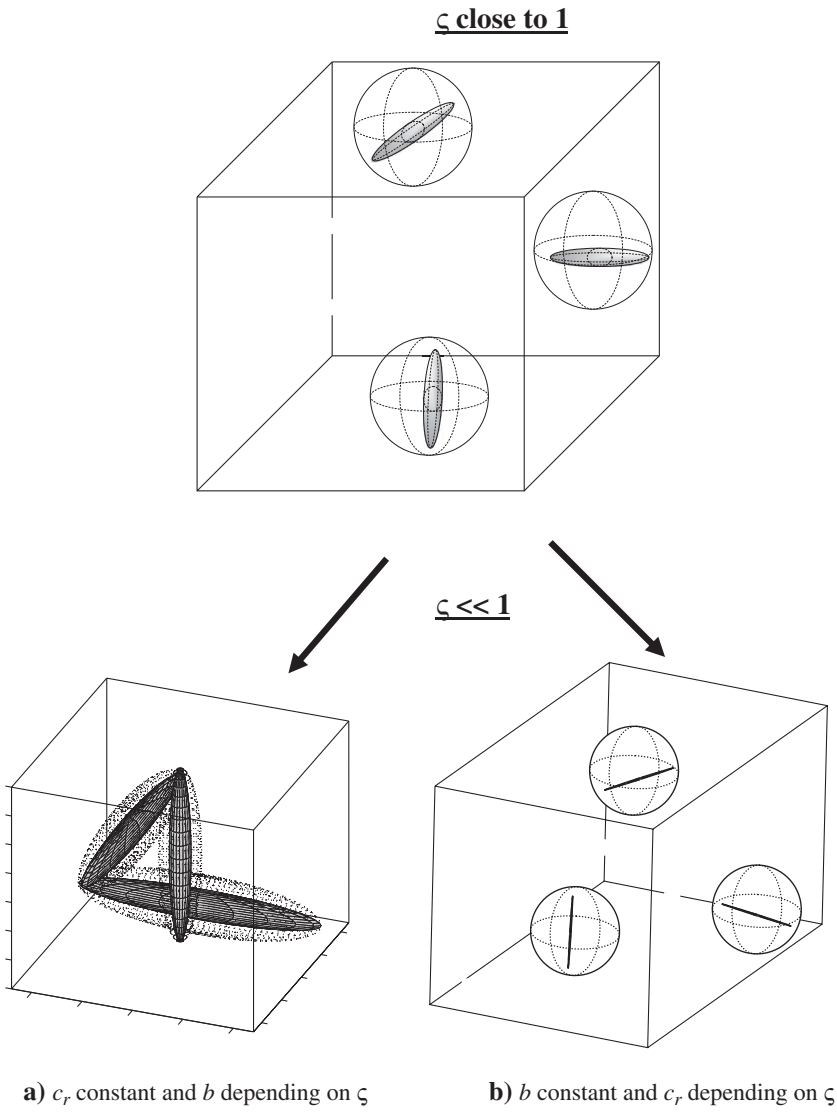

Fig. 1. Schematic representation of the evolution of the dimensions of prolate spheroids corresponding to an inclusion phase r with the shape parameter ς: (a) c_r constant ; (b) b constant.

presents the following deficiency: the spheroid maximum axis appearing on Eq. (18) has to augment, as ς decreases, and in particular tends to infinity, as ς goes to 0. The second possibility is more adapted for inclusion forms tending to cracks, but we prefer the first option, since the inclusion phases present inside the HCP are far from being crack-like. The ordinary Portland cement pastes (CEM I) with w/c=0.25, 0.40 and 0.50 used for this study are defined in Tables 1 and 2 in terms of volume fractions and mechanical properties of their constituent phases. Two examples on these materials are considered. The first one concerns the initial capillary porosity, whose concentrations are c_V=11%, 18.3% and 23.7% for w/c=0.25, 0.40 and 0.50, respectively. The effects of both types of porous spheroids on the effective Young modulus are plotted on Fig. 2 for the three CEM I pastes. These curves show that prolate and oblate porous spheroids with an identical value for the morphological parameter do not have the same effects on Young modulus except for ς close to 1. The weakening effects of prolate porous spheroids compared to the spherical case are quite negligible, whereas oblate ones have a much more pronounced impact. These tendencies are even more marked for high volume fractions of initial capillary pores. In this condition, the

Table 1
Input volume fractions of principal hydrates, unhydrated Clinker and capillary porosity for six different HCP [9]

Volume fractions in %						
w/c=	CEM I paste			CEM II/A paste		
	0.5	0.4	0.25	0.5	0.4	0.25
CH	16.4	16.9	15.7	10.5	10.8	8.5
C–S–H	47.3	47.4	42.1	49.4	49.7	45.1
UC	10.04	14.46	28	13	18.4	31.4
Aft	2.4	2.8	2.9	2.7	2.3	2.9
AFm	0.16	0.14	0.3	0.4	0.4	1
Porosity (%)	23.7	18.3	11.0	24.0	18.4	11.1

Table 2
Elastic properties of the main phases present at both levels of HCP microstructure, taken from diverse sources in the literature

Phases		Sound HCP		Leached HCP		References
		E (GPa)	ν	E (GPa)	ν	
LEVEL II	CH	**42.3**	**0.324**	**0**	**0**	[24]
		38	0.31			[2]
	Unhydrated Clinker	**117.6**	**0.314**	**117.6**	**0.314**	[3]
	Initial capillary porosity	**0**	**0**	**0**	**0**	
	AFt	**22.4**	**0.25**	**0**	**0**	[9]
		52	0.30			[25]
		25	0.25			[26]
	AFm	**42.3**	**0.324**	**0**	**0**	[9]
		22.8	0.24	22.8	0.24	[2]
	C–S–H gel	**22.4**	**0.25**	**22.4**	**0.25**	[5]

The numerical values used for the calculations are in bold.

parameter seems not to be well appropriate except for values higher than 0.80. But it should be underlined that this example corresponds to an extreme case, since the contrast between the elastic properties of matrix and inclusion is infinite.

The second example illustrates the case of finite contrast by focusing on unhydrated Clinker inclusions, which are stiffer than the C–S–H matrix. Their volume fractions in the three CEMI pastes are $c_{UC}=10.04\%$, 14.46% and 28%, respectively. The curves obtained when ς varies from 0 to 1 for both types of spheroids are presented on Fig. 3; they are relatively close and, for ς higher than 0.5, the Young moduli estimated with oblate and prolate spheroids are almost confounded. For lower values, oblate spheroids produce a stronger stiffening effect. This result is not surprising in view of the evolution of the spheroids with ς: as the latter goes to 0, oblate spheroids tend to infinite disks whereas prolate ones tend to infinite needles, as may be observed on Fig. 1. Both types of spheroids thus tend to radically different geometries. For this particular example, ς turns out to be relevant on a limited range, where it is useful for approaching real inclusion shapes. For inclusions whose geometrical shape is very aspherical, ς is small and other parameters are required to precisely characterize the effects of morphology on elastic moduli. This remark applies particularly when the contrast between matrix and inclusion elastic properties is high, as in the first example presented above.

From the microstructural description detailed in Section 2.1, it appears that needle-like Ettringite should rather be characterized by prolate shapes and disk-like Portlandite by oblate morphologies, as shown on Fig. 4. Concerning unhydrated Clinker, AFm and initial capillary pores, no evidence indicates whether to preferentially use oblate or prolate spheroids for characterizing their shape. Thus, they are represented by 50% of both oblate and prolate spheroids in this work.

3.2. Significance of the shape parameter for HCP elastic properties

The purpose of this subsection is to determine the particulate phases whose shape parameter may become significant for the estimation of elastic properties and to find some approximate values for ς on the basis of experimental observations. The influence of ς on HCP elastic properties is first studied for the level I of microstructure. Only the two inner and outer products C–S–H^{int} and C–S–H^{ext} are considered at this scale. We now make ς vary for the inclusion phase C–S–H^{int} and, hence, study its influence on C–S–H effective elastic properties in unleached and leached states. It has been observed that the amount of both

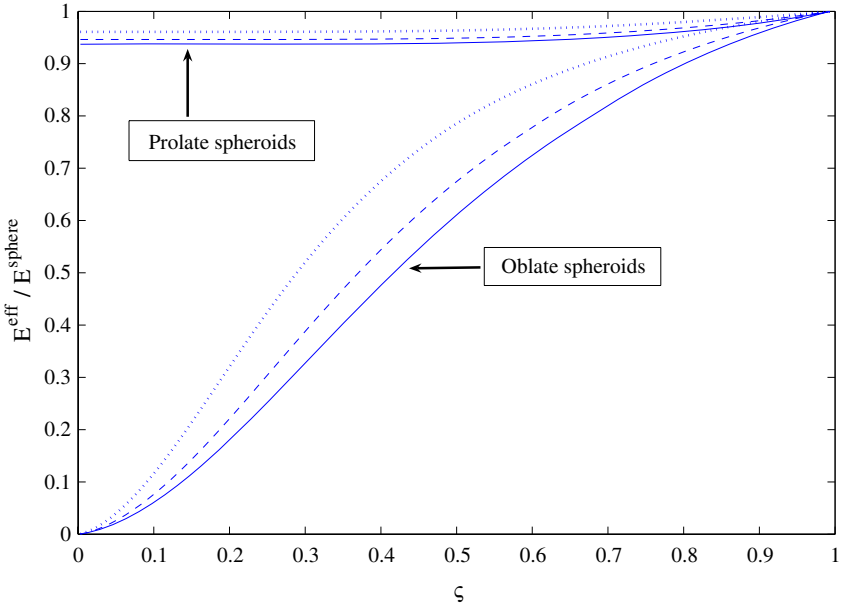

Fig. 2. Evolutions of the normalized effective Young modulus for sound CEM I pastes with capillary pores as a function of the shape parameter ς for different volume fractions. The pores are modeled as oblate or prolate spheroids, respectively illustrated under and over the curves. Solid lines: $w/c=0.5$($c_V=23.7\%$), dashed lines: $w/c=0.4$($c_V=18.3\%$), dotted lines: $w/c=0.25$($c_V=11\%$).

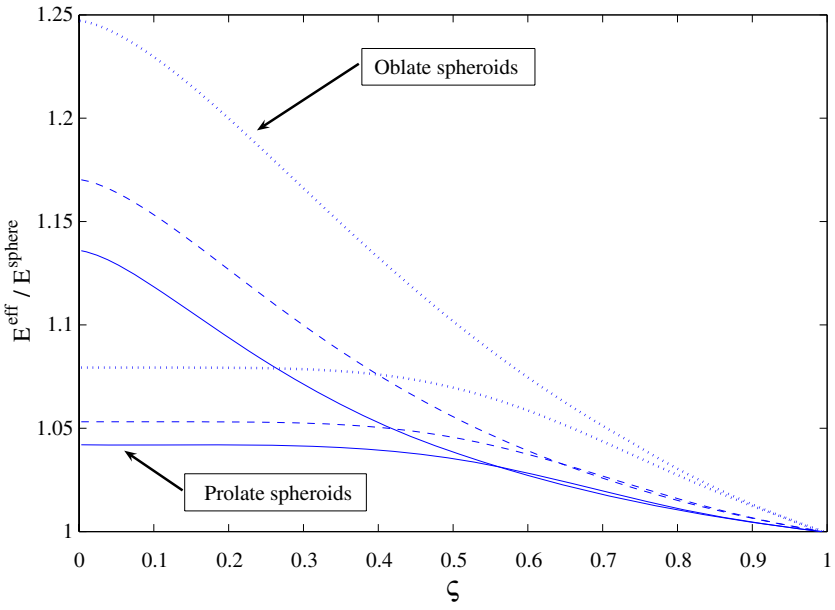

Fig. 3. Evolutions of normalized effective Young modulus for sound CEM I pastes with unhydrated Clinker respectively represented by oblate and prolate spheroids, as a function of the shape parameter ς. Solid lines: $w/c=0.5$; dashed lines: $w/c=0.4$; dotted lines: $w/c=0.25$.

C–S–H types ($c_{\text{C–S–H int}}=0.30$ and $c_{\text{C–S–H ext}}=0.70$) seems not to change when leaching occurs [2,35]. When C–S–H is subjected to decalcification, the nanoporosity in both types increases [35], but the progressive evolution of their elastic properties during the leaching process seems not to have been experimentally characterized yet. To the best of our knowledge, only the Young moduli of extremely degraded C–S–H^{ext} and C–S–H^{int} are presently known [2], diminishing from 21.7 GPa to 3 GPa and from 29.4 GPa to 12 GPa, respectively. These moduli were obtained by supposing that the Poisson ratio of both phases remains constant and equal to 0.24 [2,36]. Their bulk and shear moduli, designated by $K_{\text{C–S–H int}}$, $G_{\text{C–S–H int}}$ for C–S–H^{int} and by $K_{\text{C–S–H ext}}$, $G_{\text{C–S–H ext}}$ for C–S–H^{ext}, are immediately deduced from the following relations:

$$K_k = \frac{E_k}{3(1-2\nu)} \text{ and } G_k = \frac{E_k}{2(1+\nu)} \text{ with}$$
$$k = \left\{\text{C}-\text{S}-\text{H}^{\text{int}},\ \text{C}-\text{S}-\text{H}^{\text{ext}}\right\}$$

The input elastic parameters for the two sound phases are such that $K_{\text{C–S–H int}}=18.8$ GPa, $G_{\text{C–S–H int}}=11.9$ GPa and $K_{\text{C–S–H ext}}=13.9$ GPa, $G_{\text{C–S–H ext}}=8.8$ GPa. Their degraded elastic properties decrease to $K^l_{\text{C–S–H int}}=7.7$ GPa, $G_{\text{C–S–H int}}{}^l=4.8$ GPa and $K^l_{\text{C–S–H ext}}=1.9$ GPa, $G^l_{\text{C–S–H ext}}=1.2$ GPa (the subscript l stands for leached state). It is noteworthy to precise that all these moduli are calculated by assuming that the Poisson ratio of both phases is not sensitive to leaching [2,36]. This approximation is made due to the lack of experimental data on the Poisson ratio but requires a critical assessment. For example, it may be instructive to see what would happen if the Poisson ratios of the two leached phases were supposed to follow the same evolution as the values measured by nanoindentation, so that $\nu^l_{\text{C–S–H}}=0.034$ and $\nu^l_{\text{C–S–H ext}}=0.098$. Given that the results from nanoindentation not only depend on the Young modulus but also on the square of the Poisson ratio [4], the respective Young moduli of the leached C–S–H^{int} and C–S–H^{ext} would respectively become 12.6 GPa and 3.18 GPa with this new hypothesis. The variation of the effective Young modulus with the morphological parameter of C–S–H^{int} is plotted on Fig. 5 for both sound and degraded C–S–H matrix. The two curves obtained for the variation of the leached effective Young modulus on Fig. 5 with the different conjectures made on the Poisson ratio are still quite similar. In the ensuing, we will thus conserve for simplicity the assumption that the Poisson ratio remains unaffected by leaching [2,36]. The morphology of C–S–H^{int} is simply negligible in the sound C–S–H, since its elastic properties are very close to the C–S–H^{ext} matrix one [23]. On the opposite, the influence of C–S–H^{int} shape becomes more significant in the leached case (leading to 10% increase for ς close to 0), since the contrast between the elastic properties of the particulate phase C–S–H^{int} and the matrix C–S–H^{ext}, assumed to have an identical Poisson ratio, increases noticeably with leaching.

We now make the shape parameter vary individually for each inclusion phase present at the level II of the microstructure, while ς is kept fixed and equal to 1 for the other particulate phases. The dependence of the elastic properties on ς is thus investigated successively for all inclusion phases composing HCP in both sound and degraded pastes defined in Table 1. The Young moduli and the Poisson ratio of the hydrated phases in sound and decalcified states are indicated in Table 2 and the input elastic properties, namely the bulk and shear moduli, are obtained using Eq. (19). At level II, the influence of the shape of aluminates and Portlandite on effective elastic properties of unleached HCP is negligible as shown on Fig. 6. On the contrary, the morphology of initial capillary pores clearly plays a significant role due to the infinite contrast between matrix and porous inclusions, as already highlighted in the preceding

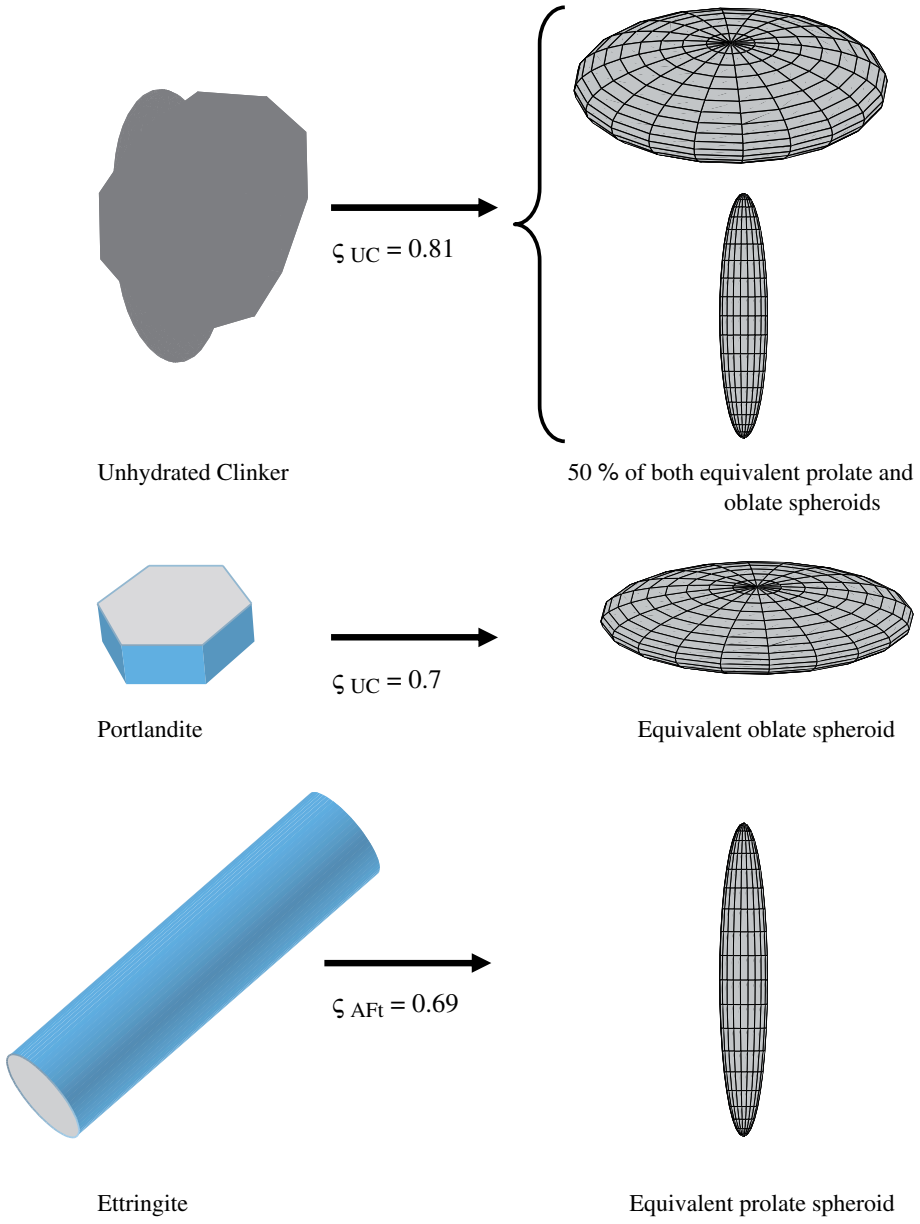

Fig. 4. Approximation of realistic HCP particulate phases shapes by equivalent spheroids.

subsection. The relative significance of this porous phase depends on its volume fraction (c_V=11%, 18.3% and 23.7% for w/c=0.25, 0.4 and 0.5, respectively). The shape of unhydrated Clinker may also have a non-negligible effect, since an increase of 25% can be obtained as ò goes to 0. A value of ς for this phase can be proposed by assuming that the Clinker residuals inherit from a shape similar to the initial cement particle one. The argument for such an assumption is that the reaction of cement particles with water initially taking place at the particle surface, the morphology of their unhydrated core should not change significantly during the hydration process. The microtomographic pictures of the evolution of cement particles morphology issued from the Visual Cement Database [17] during hydration permit to properly assess this assumption and show that the latter may be too idealistic. Nevertheless, this approximation is maintained, since the residual Clinker seems to inherit from a shape closer to unhydrated cement particles than spheres. Under this hypothesis, the unhydrated Clinker keeps the same shape parameter value as the initial cement grains: $\varsigma_{UC}=\varsigma_{\text{cement particles}}\cong 0.81$. As illustrated on Fig. 4, this particulate phase is then approximated by equivalent oblate and prolate spheroids of respective aspect ratios of r_{UC}=0.35 and r_{UC}=3.5. However, the difference between HCP effective Young moduli estimated by means of Clinker spheroidal inclusions having a shape parameter of ς_{UC}=0.81 with respect to the spherical case remains quite negligible except for high volume fractions of Clinker. This statement leads to the remarkable consequence that, though the shape of anhydrous residuals is noticeably non-spherical, it may not affect importantly the elastic properties.

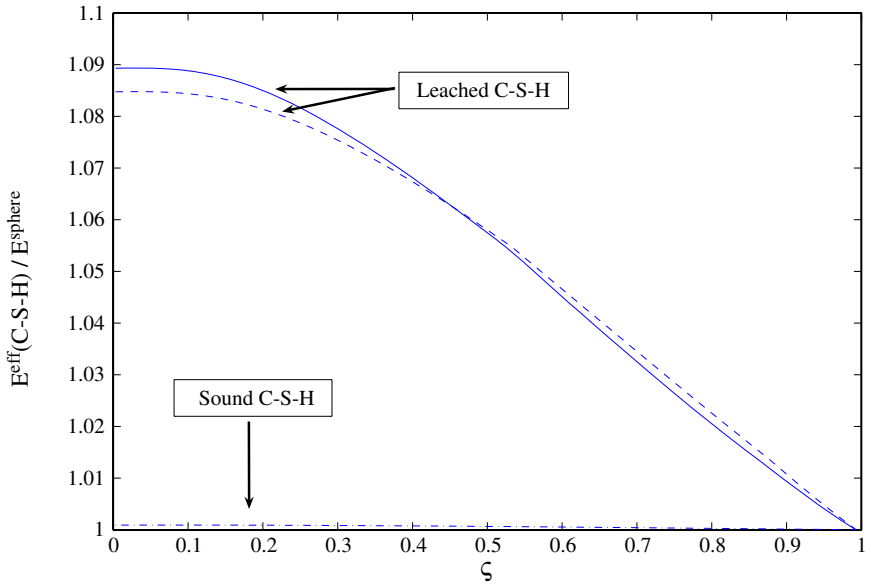

Fig. 5. Evolutions of the normalized effective Young modulus for both leached and sound C–S–H matrix, as a function of the shape parameter ς. Solid lines: leached C–S–H with Poisson ratio supposed unaffected; dashed lines: leached C–S–H with poisson ratio supposed affected; dashed-dotted lines: sound C–S–H.

We now focus on the degraded state. The degradation process retained here is briefly summarized below. CH crystals dissolve before any other hydration products during decalcification process. The C–S–H in turn is degraded but does not dissolve totally. As the leaching proceeds, the aluminate phases, AFt and AFm, are decalcified and dissolved. CH, AFt and AFm are assumed to be completely dissolved and replaced by additional capillary pores. Concerning the degraded pastes, the FE simulations presented in the next section include the leaching of CH and aluminates but do not incorporate the degradation of C–S–H [9]; we have then adopted the same leaching scenario to be able to compare the different results. Evolutions of the Young modulus as a function of ς for the three CEM I pastes when CH, AFt and AFm are degraded successively are presented on Fig. 7. The influence of leached Portlandite morphology increases considerably compared to the sound state. This is partly due to its high volume fractions (> 15%) but it should also be emphasized that its effects are even more significant than the initial capillary pores one, although some of their concentrations are higher (c_V=11%, 18.3% and 23.7%). As may be observed on Fig. 2, the decrease of the effective Young modulus is much more pronounced for oblate spheroids than for prolate ones. Consequently, the elastic properties are more sensitive to the flattened morphology of CH than to the initial capillary pores one, represented not only by oblate spheroids but also by prolate ones (see Fig. 4). For ς

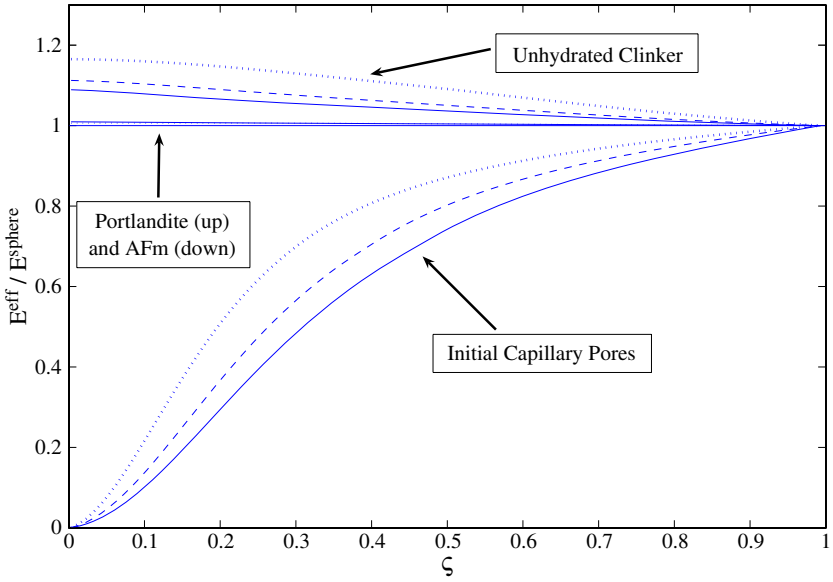

Fig. 6. Evolutions of the normalized effective Young modulus for sound CEM I pastes, as a function of the morphological parameter ς. Solid lines: w/c=0.5; dashed lines: w/c=0.4; dotted lines: w/c=0.25.

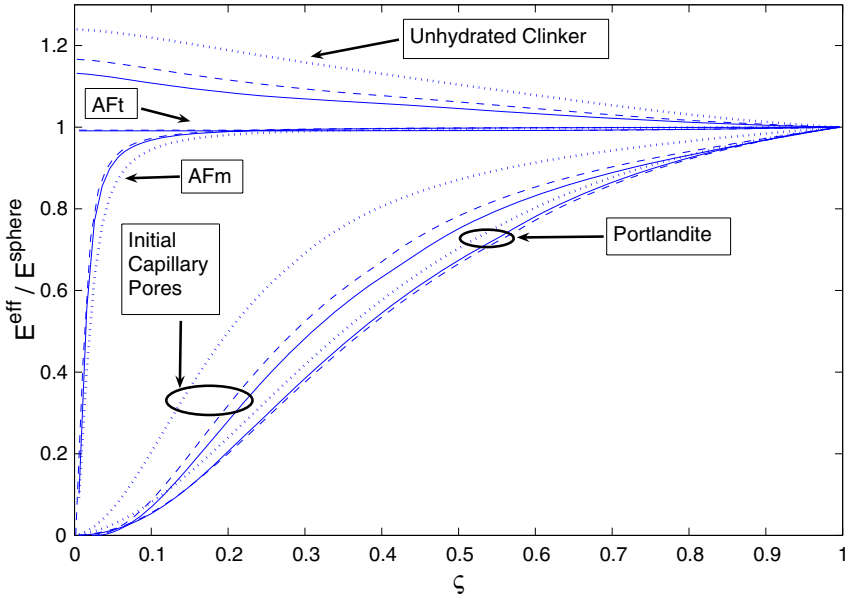

Fig. 7. Evolutions of the normalized effective Young modulus for leached CEM I pastes, as a function of the morphological parameter ς. Solid lines: $w/c=0.5$; dashed lines: $w/c=0.4$; dotted lines: $w/c=0.25$.

higher than 0.1, the influence of dissolved Ettringite and AFm shapes remains negligible because of their scarce volume fractions (see Table 1). Concerning unhydrated Clinker, the effect observed for $\varsigma_{UC}=0.81$ is still insignificant. Furthermore, some approximate values may be found for CH and AFt shape parameters. By examining carefully micrographs of Brown and Hooton [37], Ettringite is characterized by long cylinders, whose height is at least 10 times bigger than its diameter, as represented in Fig. 4. These rather empirical dimensions provide a morphological parameter $\varsigma_{AFt}=0.69$, having an insignificant influence according to Fig. 7. Portlandite is further assumed to inherit from a similar shape inside the HCP as in non-confined environments, where it crystallizes in massive hexagonal plates [13]. Considering such a plate, whose thickness is four times smaller than the maximum length of the regular hexagonal base, $\varsigma_{CH}=0.7$ is obtained (see Fig. 4). This value leads to a relative variation of Young modulus comprised between 0.75 and 0.9 for the three HCP, which is not negligible.

Because of the straightforward calculation of the Eshelby tensor for spherical inclusions [22], the spherical assumption is easy to use provided that morphology has a negligible effect. In this subsection, the influence of inclusion shapes on the effective mechanical properties is shown to highly depend on the contrast

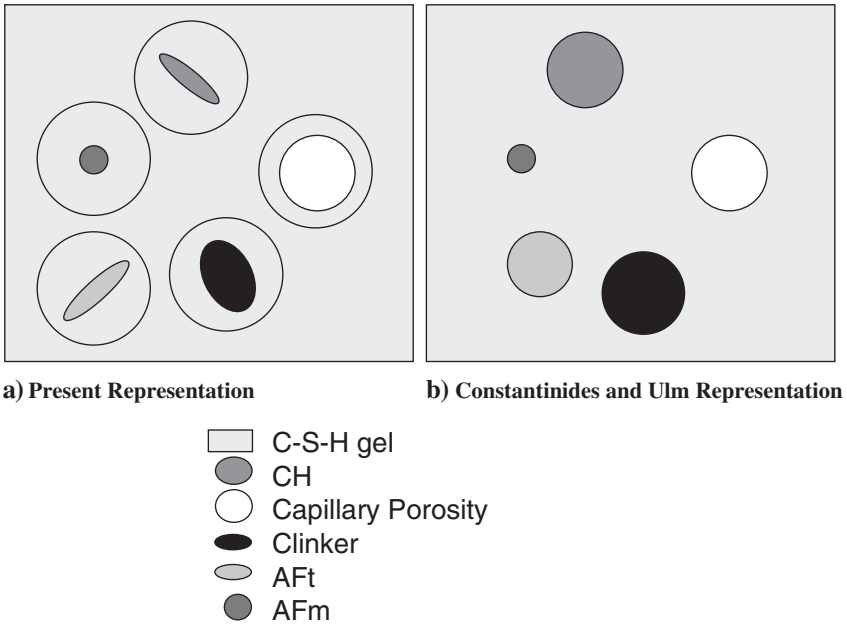

Fig. 8. (a) Two-dimensional representation of the present model based on Zheng and Du double-inclusion type scheme (left) [8]; (b) Constantinides and Ulm model (right) [2] applied to the level II of the two-step homogenization model for HCP.

between matrix and inclusion elastic parameters, on the volume fractions and on the flattening of the particles. In particular, the morphology of a completely dissolved phase such as Portlandite can severely affect the effective properties of leached HCP. Consequently, it is quite natural to wonder if the sphere really constitutes a reasonable approximation. The spheroids (see Fig. 4) chosen from experimentally based approximate values for the shape parameter of Clinker, Ettringite and Portlandite (respectively with $\varsigma = 0.81$, 0.69 and 0.7) may improve on the spherical assumption. The first value is based on the hypothesis that the residual Clinker inherits from a shape similar to the unhydrated cement particles and the last two shape parameter values are equivalent to considering the shape of CH and AFt inside the HCP identical to their well-crystallized geometry in non-confined environment. These approximations appear quite idealized in comparison with the images of [16,17] but they are probably more realistic than the spherical hypothesis. For the remaining phases, namely initial capillary pores, C–S–H^{int} and AFm, the default value taken for ς is the spherical one: $\varsigma_{Sphere} = 1$. The schematic micromechanical representation obtained with the equivalent spheroids deduced from these novel approximations is illustrated on Fig. 8a.

4. Assessment of the spherical particulate assumption

A detailed comparison with other methods applied to a representative panel of HCP is required to check the efficiency of our micromechanical estimations. In this section, we limit ourselves to the second level of HCP microstructure, where the C–S–H matrix is only regarded as a homogenized phase. The results of the Constantinides and Ulm model and the one detailed above are presented for six different HCP and also compared to FE simulations performed by Kamali [9]. Three CEM I and three blended Portland cement pastes with 7.7% silica fume content (CEM II/A) with various *w/c* ratios (0.25, 0.40, 0.50) are considered. The volume fractions and elastic properties of their elementary phases can be found respectively on Table 1 and on Table 2 for the six HCP samples in sound and degraded states. The input numerical values for the micromechanical estimations are the same as those employed by Kamali [9]. Two NIST models are used for the FE simulations [9]: CEMHYD3D and ELAS3D [38–40]. The first one is a three-dimensional cement hydration and microstructure development modeling package. The second one is a linear elastic FE program developed for computing the linear elastic properties of random materials whose microstructure has been stored in a 2D or 3D digital image. CEMHYD3D is probably the most well-known and efficient hydration model. A unit cell of 100 μm in size was used for all the simulations. The limitations of these simulations come from the size of the voxels being only of 1 μm^3. For further details, the reader should refer to the recent article of Haecker and al. [34].

Fig. 9a and b recapitulate the results obtained by the micromechanical models and numerical simulations. They suggest a few general comments. First, the Young moduli of the six HCP strongly depend on the *w/c* ratio: the value obtained for HCP with a low *w/c* ratio (*w/c* = 0.25) is about 50% higher

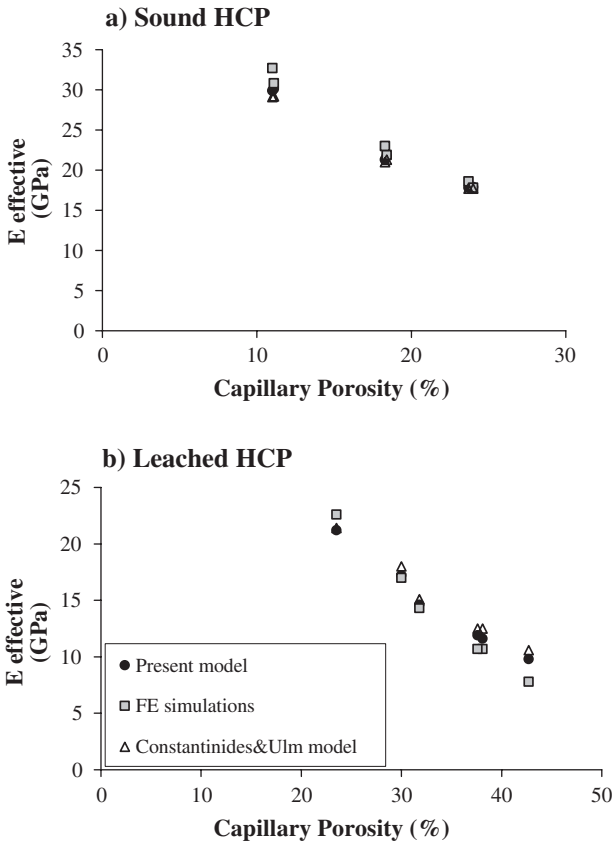

Fig. 9. (a) and (b) Evolutions of the effective Young moduli estimated by our IDD homogenization model, by Constantinides and Ulm one [2] and by FE simulations [9] for both sound and degraded HCP (whose composition is defined on Table 1), as a function of capillary porosity volume fraction.

than for a high *w/c* ratio HCP (*w/c* = 0.50). Second, the detrimental effect of leaching on Young modulus is significant though the elastic properties of C–S–H are kept constant during the degradation process. Kamali [9] predicted a reduction varying between 48% and 58% for the CEM I pastes and obtained good agreement with experimental results measured by Carde [41], where total dissolution of CH caused a reduction of 55% in the Young modulus of Portland cement paste with *w/c* = 0.5. Gallé et al. [42] measured a decrease from 23 GPa to 7 GPa (a 71% reduction) on the dynamic elastic modulus of a CEM I *w/c* = 0.45 paste subjected to a complete degradation. The numerical results of Kamali [9] agree quite well with their measures considering the fact that the paste appears more degraded in the experiments [42] than in the simulations. The decrease of the Young modulus is lower for CEM II/A pastes, varying between 25% and 40%. The blended cement pastes show better mechanical properties after degradation process than CEM I because of their small content of Portlandite. This phase appears then to be predominant for leaching problems.

For all sound pastes, the results of both micromechanical models are in good agreement with the FE values, since the deviation compared to numerical simulations is always lower than 9% for our estimate and 12% for the Constantinides and Ulm one. In view of the fact that FE simulations are more difficult to perform than an explicit homogenization method, the

latter provides an efficient analytical tool for the prediction of sound HCP elastic properties. Our model does only improve modestly on the Constantinides and Ulm one except when the concentration of unhydrated Clinker is high. These results confirm the previous curve on Fig. 6 showing that the morphologies of UC, CH and AFt do not strongly affect the effective properties of sound HCP. The present estimate becomes of higher interest for early-age cement pastes where the amount of Clinker is particularly high. Otherwise, it is perhaps not worthy to take spheroidal shapes for Clinker, Ettringite and Portlandite, the spherical assumption already giving satisfactory results.

For the leached cases, our estimations remain closer to the FE simulations than the Constantinides and Ulm effective medium approximation except for the CEM II/A $w/c=0.25$ paste but both diverge significantly from the numerical results for volume fractions of capillary porosity higher than 35%. This improvement tends to prove that the proposed approximations constitute a better alternative to the spherical assumption. More precisely, in our micromechanical representation illustrated on Fig. 8a), Portlandite, Ettringite and Clinker are no longer idealized by spheres but are presently approximated by spheroids with an appropriate shape parameter. Compared to the spherical case, the elongated spheroids of Ettringite and the flattened ones of Portlandite weaken the leached cement pastes, while those of unhydrated Clinker tend to stiffen the effective material. Fig. 7 reveals that the detrimental impact due to the oblate shape of Portlandite prevails on the stiffening effects due to the asphericity of unhydrated Clinker and leached AFt. Therefore the variations between our estimations and the Constantinides and Ulm ones are mainly due to the strong influence of leached Portlandite shape. It should be underlined that, though its shape is negligible in sound HCP, it becomes a crucial data for leached ones.

However, our model is still insufficient to predict correctly the effective elastic properties of leached HCP with high volume fractions of capillary porosity. As the material degrades, this porous phase is not only composed of the initial capillary pores but also of dissolved hydrates such as CH and AFt, whose shapes inside the HCP microstructure are difficult to describe. The shape parameter may not incorporate sufficient information on the inclusion morphology. In addition, the values of ς estimated for the residual Clinker, CH and AFt in the previous section are perhaps too approximate, even though they provide better results than the spherical one. The latter values were introduced in order to give an example illustrating the limits of the spherical particulate assumption and more precise quantitative data for the morphological parameter are necessary to build a sound homogenization model. There is presently a lack of quantitative data concerning the hydrate shapes but better estimations could be obtained by characterizing more accurately their morphologies, for example with the help of the Visual Cement Database and the shape analysis techniques developed recently [17,43]. It constitutes a promising field of investigation for future improvement of the homogenization processes.

Nevertheless, even if it were ideally possible to directly integrate the exact shapes of all elementary phases in the homogenization process, it is not guaranteed that micromechanical estimations of the effective elastic properties would be fully accurate. Indeed, MT and IDD effective medium approximations may fail to adequately account for interactions between highly concentrated porous inclusions. Berryman and Berge [44] have compared MT estimates obtained with different inclusion shapes with experimental data on porous materials such as sintered glass beads and concluded that it should not be used when the inclusion volume fraction is greater than 20–30%. Our results seem to be coherent with their analysis: the more porous the material becomes, the more MT but also IDD overestimates elastic properties.

5. Conclusion

In the present paper, the validity of the spherical inclusion approximation in the homogenization process applied to both sound and leached HCP has been assessed through the use of MT and IDD schemes. For this purpose, the estimations obtained with spherical inclusions are compared to the results of Kamali [9] by FE simulations. On the one hand, this simplification turns out to be suitable for sound pastes and the model of Constantinides and Ulm based on the MT scheme thus constitutes an excellent analytical tool for estimating their elastic properties [2]. On the other hand, our work evidences the limits of the spherical assumption for leached pastes. In addition, the inclusion shape influence on the effective elastic properties of HCP is examined by successively modeling each particulate phase as spheroids, whose shape ranges from needle-like to disk-like. The significant effects observed for the additional capillary porosity formed by leaching of hydrated products show the necessity of better approaching the morphologies of dissolved phases such as Portlandite.

Furthermore, an analytical way has been proposed to integrate more realistic inclusion morphologies in homogenization estimates. The key point of this method is the introduction of the morphological parameter ς, which corresponds to the normalized characterizations of the ratios between the volume and surface of inclusions. This parameter appears as the most important one after volume fractions. Approximate values of ς for particulate phases such as Clinker, Portlandite and Ettringite are proposed on the basis of experimental results. These phases are then represented by equivalent spheroids. This procedure allows to conveniently couple experimental observations and micromechanical modeling. The explicit micromechanical estimations thus obtained for the effective elastic properties of HCP are shown to give better results than those performed with the spherical approximation. However, they are still insufficient for degraded cement pastes with capillary porosity higher than 40%. Two reasons are possible for these shortcomings. It could first be due to intrinsic insufficiencies of the micromechanical estimate. The latter might fail to properly account for interactions between highly concentrated inclusions. Secondly, the convenient use of spheroids determined by means of the morphological parameter presents the considerable advantage of providing an analytical model but it may have its

limits to approach fairly complex shapes. Moreover, the values proposed for this parameter are very approximate due to the lack of complete morphological information on hydration products. The further development of three-dimensional image analysis methods [43] should give the opportunity to better characterize the morphology of inclusion phases, in particular for Portlandite, and might lead to improvement of homogenization methods in the field of cementitious materials durability. Future efforts are planned to gain quantitative shape data on the hydration products or the residual Clinker.

Acknowledgements

Financial support from DEN/DSNI/Réacteur is gratefully acknowledged. We also wish to thank D. P. Bentz and E. J. Garboczi for answering to my questions.

Appendix A. Non-overlapping condition and determination of the double-inclusion geometry for highly concentrated spheroidal inclusions

If an inclusion overlaps its double-inclusion, the homogenization calculations fail to work. The inclusion volume fraction c_I is represented by the ratio of inclusion volume on the double-inclusion one. When $r_I \neq 1$, the condition on volume fractions which has to be respected in order to avoid overlapping of inclusions reads [28]:

$$\begin{cases} c_{I+} = \dfrac{V_I}{V_{DI}} = r_I & (r_I < 1) \\ c_{I+} = \dfrac{V_I}{V_{DI}} = \left(\dfrac{1}{r_I}\right)^2 & (r_I > 1). \end{cases} \tag{A.1}$$

These equations express the condition for the spheroidal inclusion not to overlap the double-inclusion (see Fig. 10). The use of a spherical double-inclusion enclosing spheroids has the consequence that $c_I \leq c_{I+}$. Note that this condition is even more restrictive for prolate spheroids than for oblate ones due to the presence of the square in the expression (A.1) of c_{I+}.

For concentrations higher than c_{I+}, the double-inclusion can no longer be taken as spherical. To avoid any risk of overlap, it is sufficient to adapt its geometry to the inclusion one (see Fig. 10). Its aspect ratio r_{DI} is suitably chosen so that the IDD remains valid for any concentration as illustrated on Fig. 10.

In other words, the determination of the double-inclusion geometry is now linked to the choice of inclusion shape. The IDD estimate taken with such a shape for the double-inclusion works for any concentration and is called the full-range IDD [8].

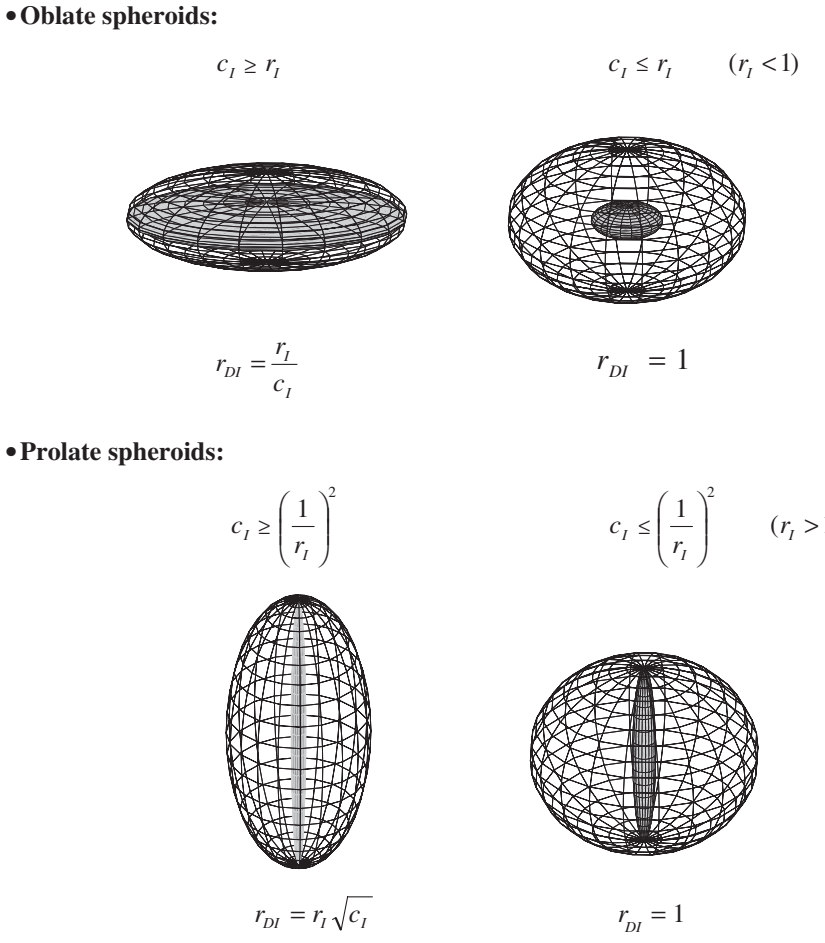

Fig. 10. Schematic illustrating the non-overlapping condition and the variation of the double-inclusion geometry with the volume fraction of a particulate phase represented respectively by oblate and prolate spheroids.

References

[1] M. Neubauer, T.B. Bergstrom, K. Sujata, Y. Xi, E.J. Garboczi, H.M. Jennings, Drying shrinkage of cement paste as measured in an environmental scanning electron microscope and comparison with microstructural models, J. Mater. Sci. 24 (1997) 6415–6427.

[2] G. Constantinides, F.-J. Ulm, The effect of two types of C–S–H on the elasticity of cement-based materials: results from nanoindentation and micromechanical modeling, Cem. Concr. Res. 34 (1) (2004) 67–80.

[3] A. Boumiz, D. Sorrentino, C. Vernet, F. Cohen Tenoudji, Modelling the development of the elastic moduli as a function of the degree of hydration of cement pastes and mortars, in: A. Nonat (Ed.), Proceedings 13 of the 2nd RILEM Workshop on Hydration and Setting, 1997, Dijon, France, RILEM Publications, France, 1997.

[4] K. Velez, S. Maximilien, D. Damidot, G. Fantozzi, F. Sorrentino, Determination by nanoindentation of elastic modulus and hardness of pure constituents of Portland cement clinker, Cem. Concr. Res. 31 (4) (2001) 555–561.

[5] D. Damidot, K. Velez, F. Sorrentino, Characterisation of Interstitial Zone (ITZ) of high performance cement by nanoindentation technique, 11th International Conference on Cement Chemistry, Durham, South Africa, 2003.

[6] J.J. Hughes, P. Trtik, Micro-mechanical properties of cement paste measured by depth-sensing nanoindentation: a preliminary correlation of physical properties with phase type, Mater. Charact. 53 (2004) 223–231.

[7] O. Bernard, F.J. Ulm, E. Lemarchand, A multiscale micromechanics-hydration model for the early-age elastic properties of cement-based materials, Cem. Concr. Res. 33 (2003) 1293–1309.

[8] Q.-S. Zheng, D.-X. Du, An explicit and universal applicable estimate for the effective properties of multiphase composites which accounts for inclusion distribution, J. Mech. Phys. Solids 49 (2001) 2765–2788.

[9] S. Kamali, Comportement et simulation des matériaux cimentaires en environnements agressifs: lixiviation et température, PhD thesis LMT-ENS de Cachan, France, 2003 (in French); S. Kamali, M. Moranville, E. J. Garboczi, S. Prené, B. Gérard, Hydrate dissolution influence on the Young's modulus of cement pastes, proceedings of the 5th international conference on fracture mechanics of concrete and concrete structures (FRAMCOS V), in: Li and al. (Eds.), Vail, USA, 2 (2004) 631–638. Also available at http://ciks.cbt.nist.gov/~garbocz/hydrate04/hydrate.htm.

[10] A. Zaoui, Matériaux hétérogènes et composites, lecture notes, Ecole Polytechnique, Paris, 1997 (in French).

[11] H.M. Jennings, A model for the microstructure of calcium silicate hydrates in cement paste, Cem. Concr. Res. 30 (1) (2000) 101–116.

[12] P.D. Tennis, H.M. Jennings, A model for two types of calcium silicate hydrate in the microstructure of Portland cement pastes, Cem. Concr. Res. 30 (6) (2000) 855–863.

[13] I.G. Richardson, The nature of the hydration products in hardened cement pastes, Cem. Concr. Compos. 22 (2000) 97–113.

[14] H.F.W. Taylor, Cement Chemistry, 2nd ed., Thomas Telford, London, 1997.

[15] B. Bary, S. Béjaoui, Assessment of diffusive and mechanical properties of hardened cement pastes using a multi-coated sphere assemblage model, Cem. Concr. Res 36 (2) (2006) 245–258.

[16] S. Diamond, The microstructure of cement paste and concrete—a visual primer, Cem. Concr. Compos. 26 (8) (2004) 919–933.

[17] D.P. Bentz, S. Mizell, S.G. Satterfield, J.E. Devaney, W. George, P.M. Ketcham, J.R. Graham, J.E. Porterfield, D.A. Quenard, F. Vallee, H. Sallee, The visible cement data set, J. Res. Natl. Inst. Stand. Technol. 107 (2002) 137–148 (See also http://www.visiblecement.nist.gov).

[18] E.J. Garboczi, J.W. Bullard, Shape analysis of a reference cement, Cem. Concr. Res. 34 (10) (2004) 1933–1937.

[19] U. Rattanasak, K. Kendall, Pore structure of cement/pozzolan composites by X-ray microtomography, Cem. Concr. Res. 5 (4) (2005) 637–640.

[20] J.D. Eshelby, The determination of the elastic field of an ellipsoidal inclusion, Proc. R. Soc. Lond., A 241 (1957) 376–392.

[21] T. Mura, Micromechanics of Defects in Solids, 2nd ed., Martinus Nijhoff, Dordrecht, The Netherlands, 1987.

[22] S. Torquato, Random Heterogeneous Materials, Springer, New-York, 2001.

[23] J.F. Douglas, E.J. Garboczi, Intrinsic viscosity and polarizability of particles having a wide range of shapes, Adv. Chem. Phys. 91 (1995) 85–153.

[24] E.J. Garboczi, J.F. Douglas, Intrinsic conductivity of objects having arbitrary shape and conductivity, Phys. Rev., E 53 (1996) 6169–6180.

[25] Y. Benveniste, A new approach to the application of Mori-Tanaka's theory in composite materials, Mech. Mater. 6 (1987) 147–157.

[26] M. Hori, S. Nemat-Nasser, Double-inclusion model and overall moduli of multi-phase composites, Mech. Mater. 14 (1993) 189–206.

[27] G.K. Hu, G.J. Weng, The connections between the double-inclusion model and the Ponte Castañeda–Willis, Mori–Tanaka, and Kuster–Toksoz models, Mech. Mater. 32 (2000) 495–503.

[28] P. Ponte-Castañeda, J.R. Willis, The effect of spatial distribution on the effective behavior of composite materials and cracked media, J. Mech. Phys. Solids 43 (1995) 1919–1951.

[29] R. Hill, Elastic properties of reinforced solids: some theoretical principles, J. Mech. Phys. Solids 11 (1963) 357.

[30] D.-X. Du, Q.-S. Zheng, A further exploration of the interaction direct derivative (IDD) estimate for the effective properties of multiphase composites taking into account inclusion distribution, Acta Mech. 157 (1–4) (2002) 61–80.

[31] G. Pólya, G. Szegö, Isoperimetric Inequalities in Mathematical Physics, Princeton University Press, Princeton, 1951.

[34] C.−J. Haecker, E.J. Garboczi, J.W. Bullard, R.B. Bohn, Z. Sun, S.P. Shah, T. Voigt, Modeling the linear elastic properties of Portland cement paste, Cem. Concr. Res. 35 (10) (2005) 1948–1960.

[35] J.J. Thomas, J. Chen, H.M. Jennings, A.J. Allen, Effects of decalcification on the microstructure and surface area of cement and tricalcium silicate pastes, Cem. Concr. Res. 34 (12) (2004) 2297–2307.

[36] C. Le Bellégo, Couplages chimie-mécanique dans les structures en béton attaquées par l'eau: Etude expérimentale et analyse numérique, PhD Dissertation, ENS Cachan, France, 2001 (in French).

[37] P.W. Brown, R.D. Hooton, Ettringite and thaumasite formation in laboratory concretes prepared using sulfate-resisting cements, Cem. Concr. Compos. 24 (2002) 361–370.

[38] D.P. Bentz, Three-dimensional computer simulation of Portland cement hydration and microstructure development, J. Am. Ceram. Soc. 80 (1) (1997) 3–21.

[39] E.J. Garboczi, Finite element and finite difference programs for computing the linear electric and elastic properties of digital images of random materials. NISTIR 6269, U.S. Department of Commerce/NIST (1998). Also available at http://ciks.cbt.nist.gov/garbocz/manual/man.html.

[40] R.B. Bohn, E.J. Garboczi, User manual for finite element and finite difference programs: a parallel version of NIST IR 6269, NIST Internal Report 6997 (2003). Also available at http://ciks.cbt.nist.gov/garbocz/nistir6997/.

[41] C. Carde, Caractérisation et modélisation de l'altération des propriétés mécaniques due à la lixiviation des matériaux cimentaires, PhD thesis, INSA de Toulouse, France, 1996 (in French).

[42] C. Gallé, H. Peycelon, P. Le Bescop, Effect of an accelerated chemical degradation on water permeability and pore structure of cement-based materials, Adv. Cem. Res. 16 (3) (2004) 105–114.

[43] E.J. Garboczi, Three-dimensional mathematical analysis of particle shape using X-ray tomography and spherical harmonics: application to aggregates used in concrete, Cem. Concr. Res. 32 (10) (2002) 1621–1638.

[44] J.G. Berryman, P.A. Berge, Critique of two explicit schemes for estimating elastic properties of multiphase composites, Mech. Mater. 22 (1996) 149–164.